New Magnetic Phases of Fe-N and Mn-Al Alloys Produced by Mechanochemical Milling

Kyu-Jin Kim, Tae-Hwan Noh and Kenji Suzuki*

Division of Metals, Korea Institute of Science and Technology,

P. O. Box 131, Cheongryang, Seoul, Korea

*Institute for Materials Research, Tohoku University, Sendai 980, Japan

(Received 19 October 1994, in final form 14 December 1994)

The structural change and magnetic properties of mechanically milled Fe-N and Mn-Al alloy powders have been investigated by XRD, TEM, VSM, Mössbauer spectroscopy and inelastic neutron scattering measurements.

During milling of γ'-Fe$_4$N powders, an fcc γ'-Fe$_4$N phase is transformed to a bct α'-Fe(N) phase by stress-induced martensitic transformation, being accompanied by an initial increase in saturation magnetization. During annealing the bct α'-Fe(N) nanocrystalline phase which is obtained by mechanical grinding for a long time, an α''-Fe$_{16}$N$_2$ phase partially appears as an intermediate phase at 673~773 K, causing an increase in saturation magnetization.

During milling of Mn-45, 70 and 85 at.% Al mixed powders, Al atoms are partially solubilized into an α-Mn phase. The Al supersaturated α-Mn-type phases change from paramagnetic to ferromagnetic : the saturation magnetization is 11 emu/g for the as-milled Mn-70 at.% Al powders. Moreover, by removing almost all Al atoms from the as-milled Mn-85 at.% Al powders using chemical leaching, the saturation magnetization increases up to 36 emu/g.

The above bct α'-Fe(N) and ferromagnetic α-Mn type alloys are the magnetic materials found for the first time, by using the present mechanochemical process.

I. Introduction

Mechanical milling is a material-synthesis process by solid-solid reaction, which was originally developed by Benjamin [1] about 20 years ago. Over the years it has been successfully used to synthesize a number of supersaturated solid solution [2], quasicrystalline [3], nanocrystalline [4] and amorphous [5] materials. So far this technique has been commonly used for preparation of amorphous metallic alloys. Milling process is relatively inexpensive and offering several possibilities of technological applications. At present, the non-equilibrium phases produced by mechanical milling are anticipated and developed in the application of various fields : especially, superconducting [6], magnetic [7] and heat-resistant [8] materials etc..

The purpose of the present work is to investigate the formation of new ferromagnetic phases in Fe-N and Mn-Al systems by mechanochemical process.

II. Fe-N alloys

Ferromagnetic iron nitride has attracted great attention as a candidate material for magnetic recording heads and magnetic recording media [9, 10,11], because of high magnetic flux and good corrosion resistance in comparison with pure iron. Recently, Komuro et al. [9] succeeded in obtaining an α''-Fe$_{16}$N$_2$ phase with high magnetic flux density (B_s) of about 2.8-3.0 T by using a molecular beam epitaxy (MBE) method. However, the mass production of such materials has been desired for various technical applications.

The γ'-Fe$_4$N powders for milling were synthesized by NH$_3$ gas flow. The mechanical grinding treatment was carried out in a vibrating ball mill under N$_2$ gas atmosphere. The structural change

and magnetic properties were observed for the milled and annealed specimens after mechanical milling.

Ⅱ. 1. Milling Effect

Figure 1 shows the Mössbauer spectra of mechanically ground (MG) γ'-Fe$_4$N powders as a function of milling time. The spectrum of as-nitrided sample mainly consists of γ'-Fe$_4$N compo-
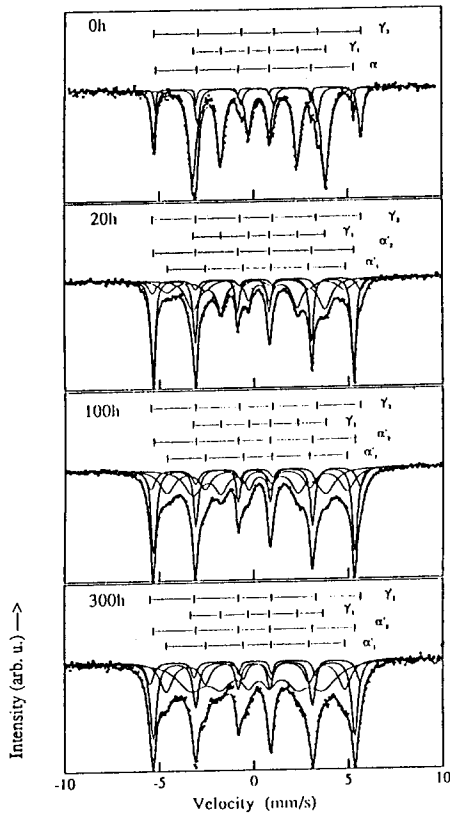

Fig. 1 Mössbauer spectra of γ'-Fe$_4$N powders as a function of milling time.

nents, γ'_1 and γ'_2, corresponding to the first and second nearest Fe sites of N atoms. At 20 h of MG, the intensity of the γ'-Fe$_4$N reduces rapidly, while the bct α'-Fe(N) components, α'_1 and α'_2, appear rapidly [12]. As shown in Table 1, their hyperfine fields are 297 and 330 kOe respectively, being allotted to the Fe sites whose 1st and 2nd

Table 1. Hyperfine parameters for the milled and annealed samples at room temperature, where H$_i$ is the manetic hyperfine field, δE the isomer shift, ΔW the line width and R. I. the percentage area of spectra.

milling time	component	H_i (kOe)	δE (mm/s)	ΔW (mm/s)	R.I. (%)
0 h	$\gamma'1$	219	0.30	0.34	69
	$\gamma'2$	342	0.22	0.18	23
	α	329	0.03	0.18	8
100 h	$\gamma'1$	217	0.30	0.44	25
	$\gamma'2$	345	0.13	0.39	7
	$\alpha'1$	297	0.17	0.33	22
	$\alpha'2$	330	0.00	0.25	46
200 h	$\gamma'1$	219	0.27	0.41	23
	$\gamma'2$	345	0.09	0.36	7
	$\alpha'1$	296	0.16	0.45	31
	$\alpha'2$	331	0.01	0.27	39
300 h	$\gamma'1$	218	0.22	0.65	18
	$\gamma'2$	345	0.06	0.21	6
	$\alpha'1$	294	0.14	0.40	34
	$\alpha'2$	331	0.02	0.27	43
673 K	$\gamma'1$	221	0.27	0.34	28
	$\gamma'2$	341	0.16	0.30	13
	α	330	0.00	0.23	35
	$\alpha''1$	303	0.01	0.46	6
	$\alpha''2$	336	−0.01	0.23	11
	$\alpha''3$	460	0.53	0.48	7
873 K	α	331	0.00	0.21	100

nearest interstitial octahedral sites are occupied by N atoms in the α'-Fe(N) phase. The line width of the α'_2 component is very narrow and similar to that of the α component for the as-nitrided sample. It indicates that the α'-Fe(N) phase is easily formed by applying a small amount of stress on the γ'-Fe$_4$N powders. However, the line width of the α'_1 component is very wide, indicating marked distribution of hyperfine field due to severe distortion in the nearest neighbor of N atoms. With further increasing milling time, the widths of α'_1 and α'_2 components become broad and their intensities increase. However, even after 300 h, the γ' component whose volume fraction is about 20 %
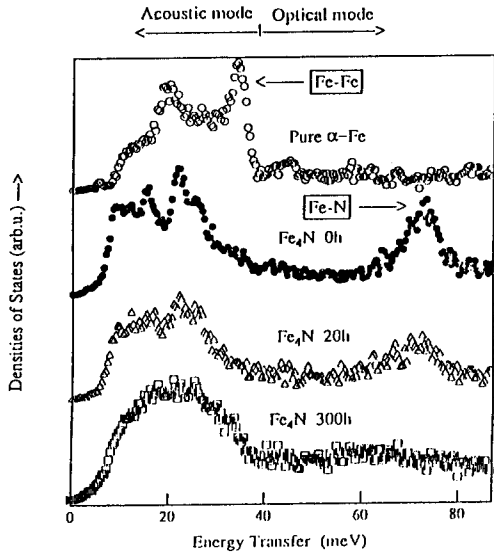
Fig. 2 Generalized phonon density of states for pure α-Fe and selectly milled γ'-Fe₄N powders.

retains.

Inelastic neutron scattering(LAM-D), installed at KENS of the National Laboratory for High Energy Physics, Tsukuba, Japan, was carried out to understand the redistribution of N atoms with milling time. The phonon densities of states, $G(\omega)$, shown in Fig. 2 for pure α-Fe and selectly milled γ'-Fe₄N powders reveal the following features.

Below 5 meV, the spectrum of the as-nitrided γ'-Fe₄N is sharper than that of pure α-Fe, indicating that the γ'-Fe₄N is elastically soft and can be easily transformed by applying smaller stress than the α-Fe. The peak above 50 meV is ascribed to Fe-N optical phonon mode. In comparison with the spectrum of the as-nitrided γ'-Fe₄N, the peak shifts to the lower energy side and its shape becomes broad with milling time. This result indicates that Fe-N bonding becomes weak and N atoms randomly diffuse into the interstitial octahedral sites of the bct α'-Fe structure.

The above martensitic transformation of the γ'-Fe₄N during milling is similar to a stress-induced martensitic transformation, but enhanced by the random diffusion of N atoms into the α'-Fe structure.

II. 2. Annealing Effect

Figure 3(a) shows XRD patterns of the 300 h-milled powders as a function of selectly annealing temperatures. Above 473 K, the α-Fe and γ'-Fe₄N
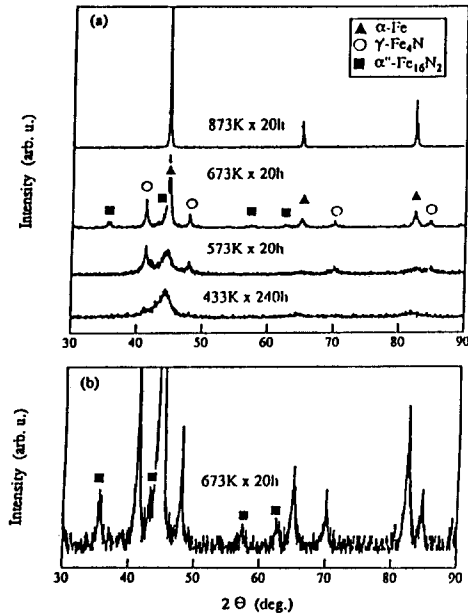

Fig. 3 (a) X-ray diffraction patterns of 300 h-milled γ'-Fe₄N powders : (a) as a function of various annealing temperatures and (b) at 673 K for 20 h.

are reprecipitated from the bct α'-Fe(N) phase. At 673 K, a new phase, which can be assigned to the α''-Fe₁₆N₂ phase in Fig. 3(b), additionally appears together with the α-Fe and γ'-Fe₄N phases. The peak positions in the XRD pattern are consistent with Jack's results [13]. On the other hand, only the α-Fe phase retains after annealing above 873 K due to the vaporization of N atoms from Fe matrix. Mössbauer spectrum in Fig. 4(a) also demonstrates the presence of the α''-Fe₁₆N₂ phase at 673 K and its volume fraction in Table 1 is 24 %. The spectrum of the α'' phase is decomposed into three components of α''_1, α''_2 and α''_3, corresponding to four Fe atoms in the 1st N nearest neighbor (n.n.) site,
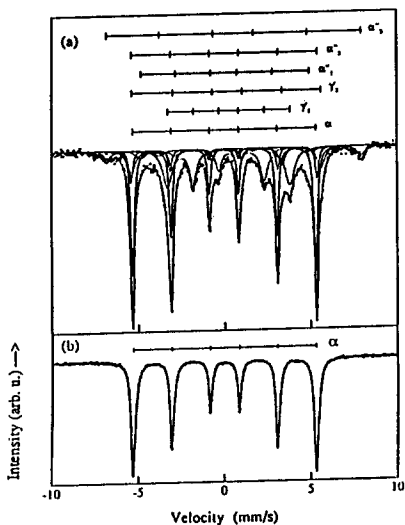
Fig. 4 Mössbauer spectra of 300 h-milled γ'-Fe₄N powders at different annealing temperatures : (a) 673 K and (b) 873 K for 20 h.

Fig. 5 Saturation magnetization, σ, and coercive force, Hc, of 300 h-milled γ'-Fe₄N powders as a function of various annealing temperatures.

eight ones in the 2nd n.n. site and four ones in the 3rd n.n. site in unit cell. Their hyperfine fields, H$_i$, are 303, 336 and 460 kOe respectively. Especially, H$_i$ of α''3 is much larger than that of the α-Fe, indicating that the magnetic moment of Fe atoms in the 3rd n. n. site is appreciably higher than that of the α-Fe. As shown in Fig. 4(b), only the α-Fe component is observed at 873 K, well corresponding to the XRD results of Fig. 4.

The saturation magnetization, σ, in Fig. 5 increases until 873 K and becomes almost constant above 873 K. Its increase is mainly caused by the formation of the α''-Fe₁₆N₂ phase below 773 K and by the vaporization of N atoms above 773 K.

III. Mn-Al Alloys

Mn is an element of 3d-transition metals which has various magnetic properties depending on its crystal structure. Pure α-Mn has a bcc structure with two clusters of 29 atoms per unit cell [14] and is stable up to 973 K. Mn atoms are distributed over four crystallographically inequivalent sites : site 1 with 2 atoms, site 2 with 8 atoms, site 3 with 24 atoms and site 4 with 24 atoms. Several neutron diffraction studies [14, 15, 16] have shown that
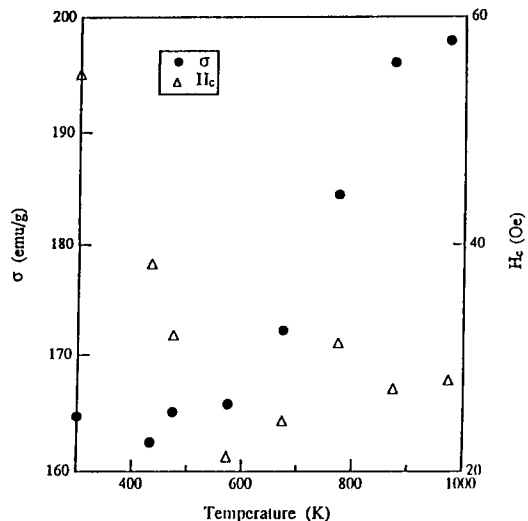
antiferromagnetism occurs below 95 K (T_N) and the magnetic moments are different at the four crystallographic sites.

Recently, Moruzzi et al. [17] and Fujii et al. [18] investigated the total-energy band calculations of α-Mn as a function of the lattice constant for paramagnetic, ferromagnetic and antiferromagnetic states. They also showed that the magnetism of α-Mn varies from a paramagnetic state through a low-spin ferromagnetic state to a high-spin antiferromagnetic state with increasing the interatomic distance.

This section discusses about the supersaturation of Al in the α-Mn phase at the viewpoint of structure and magnetic properties of milled Mn-Al alloys. By leaching out Al atoms from as-milled Mn-Al alloys, we also try to discuss about the enhancement of their magnetic properties.

Pure α-Mn and Al powders were mixed in a glove box to give a composition of Mn-45, 70 and 85 at.% Al. The mechanical alloying treatment was carried out in a rod-mill with the rotation speed of 100 rpm under 2×10^{-4} Torr state. The

rod-to-powder weight ratio was 23 : 1. The leaching treatment of Mn-Al alloys by KOH solutions leads to removal of the major portion of Al and retains 'α-Mn skeleton'.
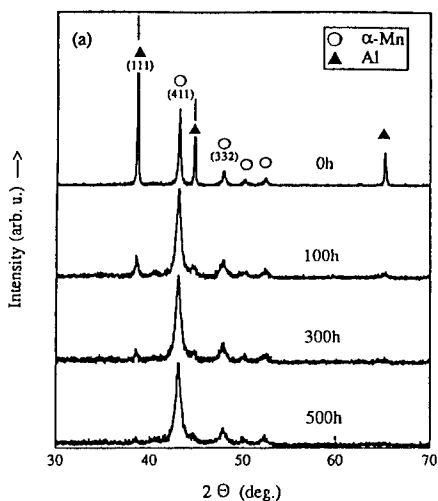

Fig. 6 X-ray diffraction patterns of Mn-45 at.% Al mixed powders as a function of milling time.

Ⅲ. 1. Milling Effect [19]

Figure 6 shows X-ray diffraction patterns of mechanically alloyed (MA) Mn-45 at.% Al powders as a function of milling time. At the initial stage of MA, Al atoms dissolve rapidly into the α-Mn phase, because the α-Mn peaks become dominant after 300 h.

Figure 7(a) shows the changes in saturation magnetization, σ, and coercive force, H_c, for variously milled samples. After 100 h, σ rapidly increases from 0 to 4 emu/g and then becomes constant, even though the α-Mn phase does not transform to another phase. H_c also increases rapidly up to 130 Oe after 100 h, due to the increase in the stored strain and Al solution. The hysteresis curve of the 100 h-milled sample in Fig. 7(b) shows ferromagnetic characteristic, which σ is supersaturated at about 3 kOe.

Figure 8 shows σ and H_c of the 300 h-milled Mn-45, 70 and 85 at.% Al powders. σ increases with increasing Al composition and represents the
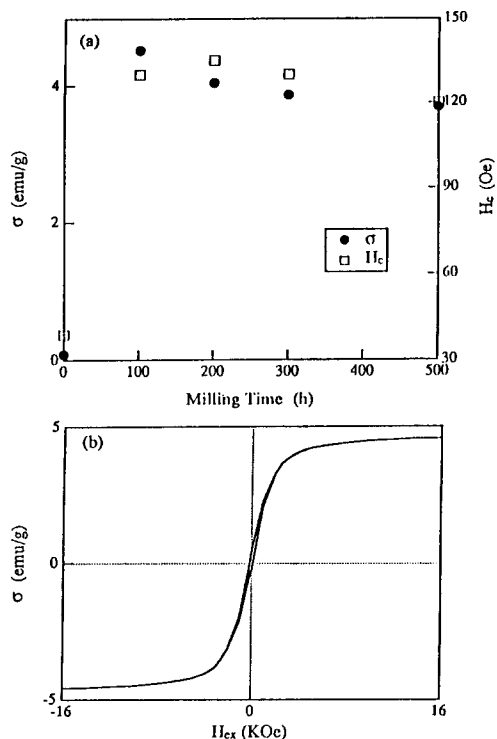

Fig. 7 (a) Saturation magnetization, σ, and coercive force, H_c, of Mn-45 at.% Al mixed powders as a function of milling time and (b) hysterisis curve of 100 h-milled Mn- 45 at.% Al alloy powder.
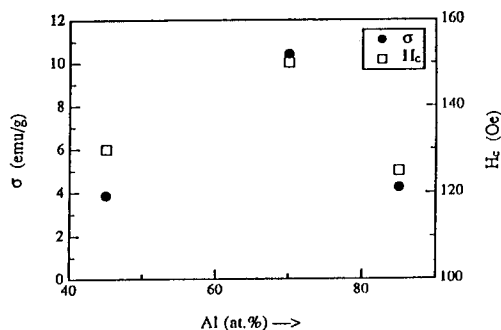

Fig. 8 Magnetic properties (σ, H_c) of 300 h-milled Mn-45, 70 and 85 at.% Al alloy powders.

maximum value of about 11 emu/g around 70 at.% Al. H_c shows the similar tendency to σ. The exist
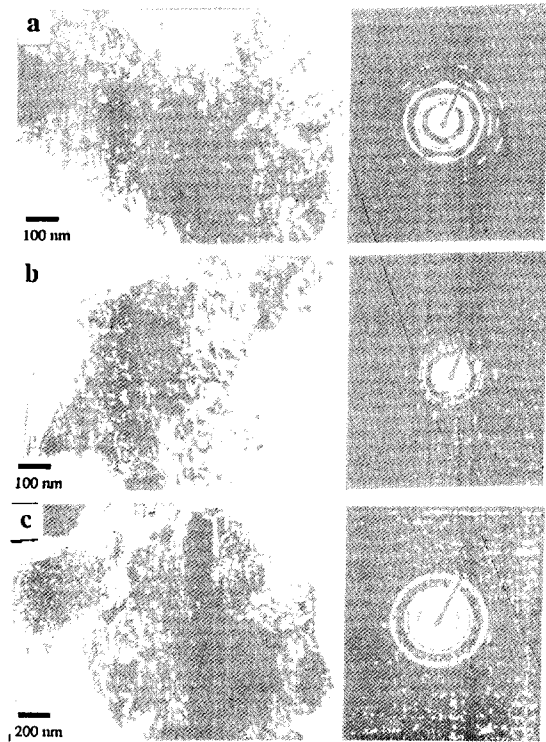
Fig. 9 Transmission electron micrographs and the corresponding diffraction patterns of (a) pure α-Mn, (b) 300h-milled Mn-85 at.% Al and (c) leached α-Mn type powders for 300h-milled Mn-85 at.% Al powders.

ence of this ferromagnetic α-Mn type alloy has not yet understood. The following factors are candidates to explain the ferromagnetism.

(1) The substitution effect of Al atoms into the α-Mn matrix partially destroys antiferromagnetic arrangement and forms ferromagnetic clusters. Such ferromagnetic clusters increase with increasing the Al substitution. However, they decrease in the Al rich alloys, due to the decrease of Mn atoms.

(2) Any marked shifts of α-Mn diffraction peaks have not been observed in the XRD patterns. However, if a microscopic displacement is generated by Al substitution into the α-Mn phase, a ferroma-

gnetism is induced at elastically expanded regions, as Kasper et al. [15] and Fujii et al. [18] have predicted.

(3) A local environment effect [20, 21] can be stated. If magnetic moments of Mn atoms are influenced by the number of Al atoms at their near neighbor sites, a ferrimagnetic states can be realized as observed in ε-Mn$_4$N [22, 23].

III. 2. Chemical Leaching Effect

Recently, Ivanov et al. [24] suceeded to produce bcc Ni by leaching Al from mechanically alloyed bcc Ni-Al powders. The Al leaching method is also applied to the as-milled Mn-85 at.% Al powder. Figure 9 shows TEM microstructures and the corresponding diffraction patterns for pure α-Mn and the as-milled and Al leached samples of Mn-85 at.% Al powders. The microstructure of the Al-leached sample shows a skeleton-type structure having many pores due to the removal of Al atoms. The corresponding diffraction pattern demonstrates only presence of the α-Mn phase. According to the EPMA analysis, the Al content in the Al leached sample is much less than that of the as-milled samples : about 95 % of Al content are
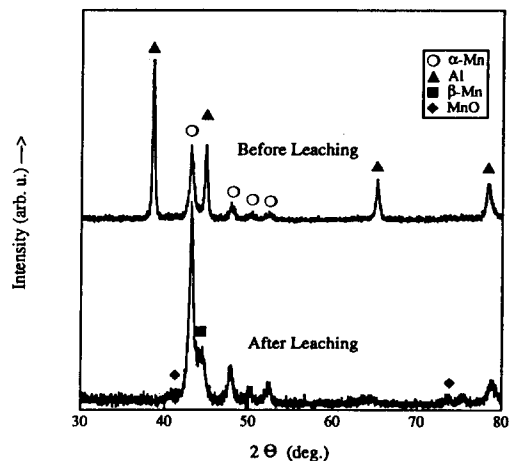

Fig. 10 X-ray diffraction pattern of leached α-Mn type powder of 300 h-milled Mn-85 at.% Al powder.

removed by leaching. In XRD patterns shown in Fig. 10, very strong Al peaks for the as-milled

sample completely disappear after leaching : strong α-Mn peaks, weak β-Mn ones and very weak MnO ones are observed in the leached sample. β-Mn is

Table 2. Magnetic properties of leached α-Mn type powder in the as-milled Mn-85 at.% Al alloy powders

samples	σ (emu/g)	H_c (Oe)
before leaching	4.3 (0.16 μB/Mn)	120
after leaching	36.0 (0.39 μB/Mn)	95

formed by the reaction of α-Mn and Al, while MnO by the reaction of α-Mn and KOH solution during leaching at 353 K. As shown in Table 2, σ of the leached sample represents 36 emu/g at room temperature. This value is 8 times larger than that of the as-milled sample, but Hc decreases 95 Oe. The remarkable increase of σ in the leached sample can not be explained only by the amount of Al removed from the as-milled Mn-85 at.% Al alloy : only about 12 emu/g increase in σ is expected by the removal of 85 at.% Al content in the as-milled sample. Since MnO phase has been known to be antiferromagnetic, it does not yield the increase of σ [25]. H atoms are solubilized in the α-Mn phase during leaching and may affect the magnetic properties of leached sample. However, its effect is not large : the maximum value of σ in MnH$_{0.94}$ phase is about 2 emu/g [26]. Therefore, the remarkable increase of σ in the leached sample is intrinsic for the leached α-Mn phase.

IV. Summary

By using milling process, several non-equilibrium phases are produced in the Fe-N and Mn-Al systems : i. e. bct α'-Fe(N) and Al supersaturated ferromagnetic α-Mn phases. These phases are formed by mechanically driven processes, accompanied by the increase of stored strain and defects during mechanical milling. The main results can be summarized as follows.

(1) In the milled γ'-Fe$_4$N powders, fcc γ'-Fe$_4$N is initially transformed into the bct α'-Fe(N) struc-

ture. This transformation is classified as a stress-induced martensitic transformation, being enhanced by diffusion of N atoms into the bct structure.

By annealing the finally milled powders, the γ'-Fe$_4$N is reprecipitated above 473 K and the α''-Fe$_{16}$N$_2$ is formed together with γ'-Fe$_4$N above 673 K, causing an increase of σ.

(2) In the milled Mn-45, 70 and 85 at.% Al powders, Al atoms are partially solubilized into α-Mn phase. The Al supersaturated α-Mn phases represent ferromagnetism and σ shows 11 emu/g at the composition of 70 at.% Al.

According to Al leaching from the as-milled Mn-85 at.% Al powder, σ increases up to 36 emu/g and this value is about 8 times larger than that of the as-milled sample.

References

1. J. S. Benjamin, Scient. Am., May (1976) 40.
2. K. J. Kim, K. Sumiyama and K. Suzuki, J. Non-Cryst. Sol., in press.
3. U. Mizutani, T. Takeuchi, T. Fukunaga, S. Murasaki and K. Kaneko, J. Mater. Sci. Lett., **12** (1993) 629.
4. M. Oehring and R. Bormann, Mater. Sci. Eng., **A134** (1991) 1330.
5. K. J. Kim, M. S. El-Eskandarany, K. Sumiyama and K. Suzuki, J. Non-Cryst. Sol., **155** (1993) 165.
6. A. Inoue and T. Masumoto, Bull. Jpn. Inst. Met., **27**, 10 (1988) 816.
7. K. Schnitzke, L. Schultz, J. Wecker and M. Katter, Appl. Phys. Lett., **57** (1990) 2853.
8. S. Shiga, T. Itsukaichi, M. Umemoto and I. Okane, J. Jpn. Soc. Powder and Powder Metall., **38** (1991) 976.
9. M. Komuro, Y. Kozono, M. Hanazono and Y. Sugita, J. Appl. Phys., **67**, (1990) 5126.
10. S. K. Chen, S. Jin, G. W. Kammlott, T. H. Tiefel, D. W. Johnson and E. M. Gyorgy, J. Magn. Magn. Mater., **110**, (1992) 65.
11. Y. Sugita, K. Mitsuoka, M,Komuro, H.

Hoshiya, Y. Kozono and M. Hanazono, J. Appl. Phys., **70** (1991)1578.

12. K. J. Kim, K. Sumiyama, K. Shibata and K. Suzuki, Mater. Sci. Eng., **A181** (1994) 1272.

13. K. H. Jack, Proc. Roy. Soc., **A208** (1955) 216.

14. C. G. Shull and M. K. Wilkinson, R. V. Mod. Phys., **25** (1953) 100.

15. J. S. Kasper and B. W. Roberts, Phys. Rev., **101** (1956) 537.

16. T. Yamada, N. Kunitomi, Y. Naki, D. E. Cox and G. Shirane, J. Phys. Soc. Jpn., **28** (1970) 615.

17. V. L. Moruzzi, P. M. Marcus and P. C. Pattnaik, Phys. Rev., **B37** (1988) 8003.

18. S. Fujii, S. Ishida and S. Asano, J. Phys. Soc. Jpn., **60** (1991) 1193.

19. K. J. Kim, K. Sumiyama and K. Suzuki, J.

Alloys and Compounds, in submitted.

20. G. G. Low. Adv. Phys., **XVIII** (1968) 371.

21. J. Friedel and C. M. Sayers, J. de Physique, **38** (1977) 697.

22. R. Juza, H. Puff and F. Wagenknecht, Z. Elektrochem., **61** (1957) 804.

23. W. J. Takei, G. Shirane and B. C. Frazer, Phys. Rev., **119** (1960) 122.

24. E. Ivanov, S. A. Makhlouf, K. Sumiyama, H. Yamaguchi and K. Suzuki, J. Alloys and Compounds, **185** (1992) 27.

25. C. G. Shull and J. S. Smart, Phys. Rev., **76** (1949) 1256.

26. I. T. Belash, B. K. Ponomarev, V. G. Tissen, N. S. Afonokova, V. Sh. Shekhtman and E. G. Ponyatovskii, Sov. Phys. Sol. State, **20** (1978) 244.

기계적 밀링 및 화학적 추출법에 의해 제조한 Fe-N 및 Mn-Al계의 새로운 자성재료

김 규진, 노 태환

한국과학기술연구원 금속연구부, 서울 136-791

Kenji Suzuki*

*Institute for Materials Research, Tohoku University, Sendai 980, Japan

밀링 및 화학적 처리에 의해 제조된 소재의 구조해석 및 자기적 특성은 X선회절, 투과 전자현미경, 뫼스바우어 분광 및 비탄성 중성자산란 등의 측정에 의해 조사되었다.

질화처리에 의해 제조된 γ'-Fe$_4$N분말의 기계적 밀링처리에 의해, 대부분의 fcc γ'-Fe$_4$N상은 밀링 초기단계에 bct α'-Fe(N)상으로 변태를 하며, 이러한 변태는 응력유기 마르텐사이트 변태로 규정지을 수 있다. 밀링처리에 제조한 bct α'-Fe(N) 초미세 분말의 열처리에 의해 673~773 K의 온도범위에서 α''-Fe$_{16}$N$_2$상이 부분적으로 생성되며, 이로 인해 포화자화값이 증가한다.

Mn-45, 70, 85 at.% Al의 조성으로 혼합한 분말은 기계적 합금화에 의해, Al은 부분적으로 α-Mn상에 고용된다. 이로 인해 α-Mn형 Mn-Al합금의 자기적 성질은 상자성에서 강자성으로 특성이 변하며, 특히 밀링처리한 Mn-70 at.% Al 계에 있어서 포화자화값은 11 emu/g을 나타낸다. 한편, 밀링처리한 Mn-85 at.% Al계에서 화학적 추출법을 이용하는 것에 의해 skeleton-type의 순 α-Mn분말상을 제조한 결과 포화자화값은 36 emu/g으로 급격히 증가하였다.